Computational Materials Science 49 (2010) 209–216

Contents lists available at ScienceDirect

Computational Materials Science

journal homepage: www.elsevier.com/locate/commatsci

Prediction of abnormal grain growth during high temperature treatment

J. Rudnizki *, B. Zeislmair, U. Prahl, W. Bleck

Department of Ferrous Metallurgy, RWTH Aachen University, Intzestr. 1 D-52072 Aachen, Germany

ARTICLE INFO

Article history:
Received 10 February 2010
Received in revised form 9 April 2010
Accepted 13 April 2010
Available online 2 June 2010

Keywords:
High-temperature carburising
Abnormal grain growth
Phase-field simulation
Zener force
Precipitates

ABSTRACT

As carburisation is a time-consuming process, it might seem advisable to shorten the process by increasing the carburising temperature. Although there is an economic advantage to high-temperature carburisation, this process is not widespread because of the problem of abnormal grain growth. Conventional case-hardening steels show heavy grain coarsening at temperatures higher than 1000 °C. To counter this problem, microalloying elements such as Nb and Ti are commonly added to resist austenite grain growth at high process temperatures. However, abnormal grain growth may still occur even when microalloying is employed. In order to gain a clearer overview about the conditions leading to abnormal grain growth, a grain growth model was developed by means of numerical simulation, using as a basis initial grain size and pinning force, which is a function of size and the volume fraction of precipitates. Finally, a threshold for initial austenite grain size and pinning force is determined, marking the change in character of grain growth in such a way that it is possible to identify optimal parameters for avoiding abnormal grain growth.

1. Introduction

Grain growth is a diffusion-controlled process driven by the reduction in grain boundary energy of a polycrystalline material as the grain size is increased. The driving force P_G for motion of a spherical curved element of grain boundary and consequently for the grain growth is inversely proportional to the radius of curvature ρ^* [1]:

$$P_G = 2\sigma/\rho^* \tag{1.1}$$

where σ is the interfacial energy. Grain growth can be inhibited in the presence of second-phase particles [2]. The retaining force executed by the precipitates is called Zener force, P_Z (1.2). This pinning force depends on the radius of precipitates and the volume fraction of the precipitate phase [3,4]:

$$P_Z = 3\sigma\frac{f}{2r} \tag{1.2}$$

where r is the radius of precipitates, f is the volume fraction of precipitate phase determined from experiments or simulations, and σ is the interfacial energy between matrix and precipitates.

The balance between the Zener force and the driving force decides whether the grain boundary is pinned or grain coarsening occurs. If the Zener force is bigger than the driving force, the grain boundaries are pinned by particles and the grain size is kept stable. In the opposite case, the grain boundaries become unstable and as pinning force decreases, grain growth can take place [5].

In general, one differentiates between two kinds of grain coarsening: normal and abnormal grain growth. During normal grain growth, all grains grow roughly at the same rate. The grain structure changes in a rather uniform way. There is a relatively narrow range of grain sizes and shapes, and the form of the grain size distribution is usually independent of time.

Abnormal grain growth characteristically involves the rapid growth of relatively few grains in an otherwise unchanged matrix [6,7]. It can be caused by anisotropy in grain boundary energy [8], anisotropy in grain boundary mobility [9] or by second-phase particles [10]. In the presence of precipitates, abnormal grain growth may take place when the pinning force has a value just slightly below the barrier making the grain boundary stabile. Due to a local gain, one local grain boundary overcomes the pinning effect, grows slightly and gets more neighbours, which strengthens the local grain boundary mobility and leads to a self-acceleration of the single-grain growth effect. The reason for this phenomenon is that the grain boundary reduces its area by moving in the direction of the curvature centre. Therefore, grains that gain in size grow further from morphological reason while the surrounding grain arrangement stays stable in size [11].

The focus of this paper is on simulating grain growth during high-temperature carburising. By means of modelling, the constraints for normal and abnormal grain growth are demonstrated.

* Corresponding author. Tel.: +49 0 241/80 90123; fax: +49 0 241/80 92253.
E-mail address: jenny.rudnizki@iehk.rwth-aachen.de (J. Rudnizki).

0927-0256/$ - see front matter © 2010 Elsevier B.V. All rights reserved.
doi:10.1016/j.commatsci.2010.04.015

2. Description of the model

Grain growth is described by phase-field simulation by means of the commercial software MICRESS® [12]. The phase-field approach was developed for modelling phase transformations in multi-component systems. It allows the calculation of a transformed phase fraction as well as a description of the microstructure evolution [13,14]. In this approach, every single-grain in the microstructure is represented by the phase-field variable ϕ_i. For the grain i, ϕ_i equals 1 in its bulk, and 0 when it is not present. On the boundary between grains i and j, $\phi_i + \phi_j = 1$. Thus, in this diffuse boundary, a material point belongs partly to the one and other grain. For grain growth, where the driving force is only the minimisation of the surface energy, the evolution of the phase-field that represents the microstructure is described by the simplified [15].

$$\frac{\partial \phi_i}{\partial t} = \sum_j M_{ij}\sigma_{ij}\left[\left(\varphi_j \nabla^2 \varphi_i - \varphi_i \nabla^2 \varphi_j\right) + \frac{\pi^2}{2\eta^2}(\varphi_i - \varphi_j)\right] \tag{1.3}$$

where M_{ij} is the interface mobility of adjacent phases and σ_{ij} is the interfacial energy. The grain growth process is controlled by the product of interfacial energy and the curvature term, which relies on microstructure description.

With respect to the Zener force, a phase-field approach can be applied to the simulation of the kinetics of grain growth in the presence of second-phase particles [15,16]. As nanosized microalloying precipitations are an effect on a scale below the micrometer scale, where grain growth takes place, the Zener force is treated as an effective entity that is assumed to be a constant value for the whole phase-field calculation area. Beside the pinning force, to the important input data for such simulations belongs grain boundary mobility, the interfacial energy, the graphical description of the microstructure. In this study, the mobility for the austenite grain boundary at 1050 °C is set to 0.71×10^{-4} cm^4/Js and the interfacial energy to 0.70×10^{-4} J/cm^2 according to [17]. The definition of the initial microstructure is a critical factor. Depending on the selected initial structure, the phase-field simulation can develop completely different results. A real structure is inhomogeneous and often contains fine as well as coarse grains in coexistence. As abnormal grain growth is a localized phenomenon, it is not easy to find the exact grain formation in the real microstructure that causes abnormal grain growth behaviour without in-situ measurements. Because fine-grain agglomerations with a critical radius of curvature can produce abnormal grain growth, one fine artificial microstructure was established for the calculations (Fig. 1).

It should be also mentioned that the cell dimension was set to 0.2 μm and the interface thickness was taken to be five cells. To analyse grain size distribution in calculated structures, the linear intercept method was used in accordance with an experimental procedure in which the third cell of each interface was assumed to be the grain boundary.

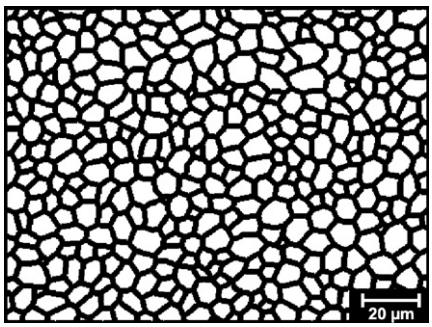

Fig. 1. Created initial microstructure with 384 grains, mean grain diameter of 7.3 μm.

3. Numerical simulation

To determine the influence of the initial microstructure and the precipitates on grain size evolution during carburising, several parameters were varied in the simulation. Figs. 2–4 present examples of microstructure evolutions based on the initial microstructure (Fig. 1), simulating carburisation at 1050 °C with a varied pinning force of 0.020, 0.060 and 0.080 J/cm^3.

Fig. 2 reveals normal grain growth. After 20 min, a uniform structure with the average grain size of approximately 20 μm was achieved; afterward, no significant changes in the structure took place, due to the fact that the driving force for the grain growth became low because of large radius of curvature and therefore, grain diameter. In contrast, Fig. 3 illustrates abnormal grain growth, where few grains grew at the expense of adjacent grains. In Fig. 4, only small changes in the initial structure were noticeable after 60 min.

The shift from normal to abnormal and no-grain growth during the increase of pinning force is demonstrated by comparing grain size distributions. Fig. 5 represents the grain size distributions for pinning forces between 0.020 and 0.035, as well as between 0.065 and 0.080 J/cm^3, illustrating the regions, where change in grain growth character takes place. At first view, the grain size distributions for the low and high pinning forces are in completely different ranges. The average grain size for the pinning force between 0.020 and 0.035, is about 25 μm, indicating a normal grain growth regime. However, for the pinning forces between 0.065 and 0.080 J/cm^3, the average grain size is about 8 μm, which fits into the no-grain growth region. Here, the grain structure is completely pinned by precipitates. Moreover, during the transition to abnormal grain growth from the normal and no-grain growth regimes, deviations from the linear slope of cumulative frequency can be observed. Thus, the deviation from the linear slope can be interpreted as a change in the grain growth character and therefore, potentially appear as abnormal grain growth. The first deviation from the linear slope is achieved at 0.030 and 0.070 J/cm^3. In contrast, at 0.025 and 0.075 J/cm^3, there is no trend of change in the grain growth character; therefore, these points can be selected as limits for the regions that are safe from abnormal grain growth.

In the next step, initial structures with average grain sizes of 10, 12.3, 14.2 and 16 μm were created on the base of the initial structure (Fig. 1) to investigate the influence of initial grain size. All results of the simulations at 1050 °C after 60 min are integrated in a diagram (Fig. 6). The grain growth character of each simulation was assigned by means of the aforementioned method, and the lines distinguishing among the three regions of normal, abnormal and no-grain growth were plotted. Thus, in this grain growth map, the dependency of the type of grain growth on the initial austenite grain diameter and pinning force is demonstrated. The lower and upper boundaries distinguish the area of abnormal grain growth affected by the combination of a critical pinning force and a critical initial grain diameter. The curve in between reflects the most critical constellation of initial austenite grain diameter and pinning force.

Although the abnormal grain growth in the structures with large initial grain sizes was not as distinctive as in structures with small initial grain sizes (due to the driving force for the grain growth, which becomes smaller with increasing radius of curvature), it is possible to determine, where abnormal grain growth takes place in relation to the initial grain size and the pinning force.

4. Comparison of simulated and experimental results

Additional simulations for the detailed investigation of abnormal grain growth were performed for two selected steels,

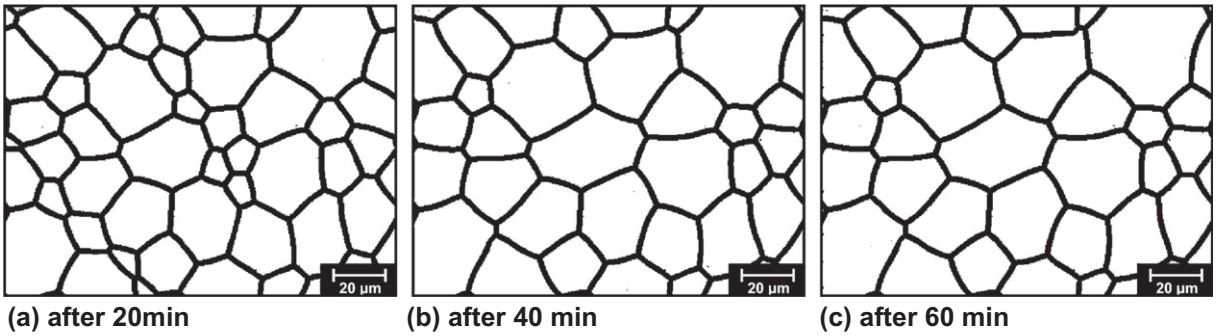

Fig. 2. Evolution of the microstructure, pinning force of 0.020 J/cm^3.

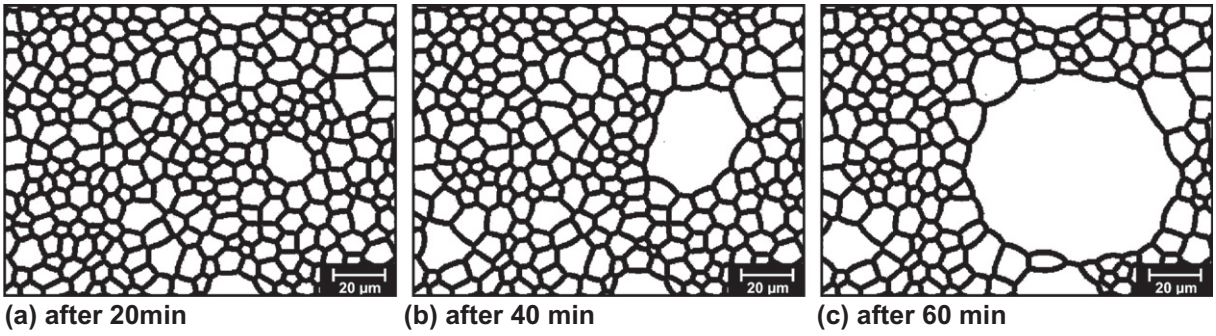

Fig. 3. Evolution of the microstructure, pinning force of 0.060 J/cm^3.

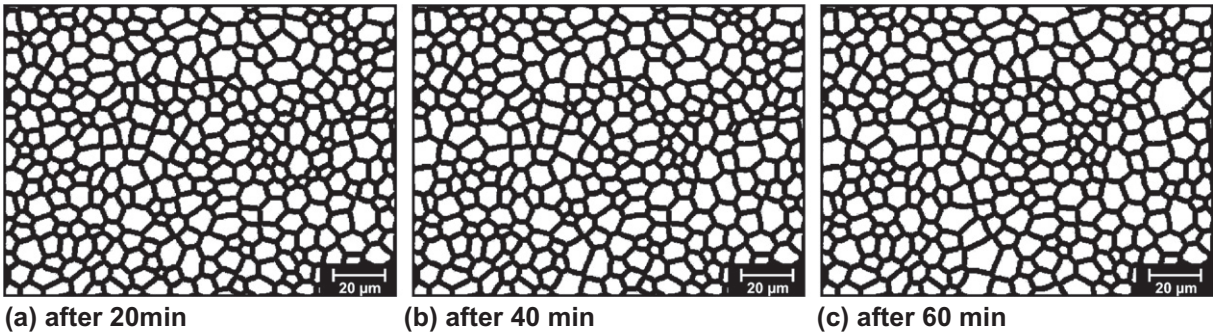

Fig. 4. Evolution of the microstructure, pinning force of 0.080 J/cm^3.

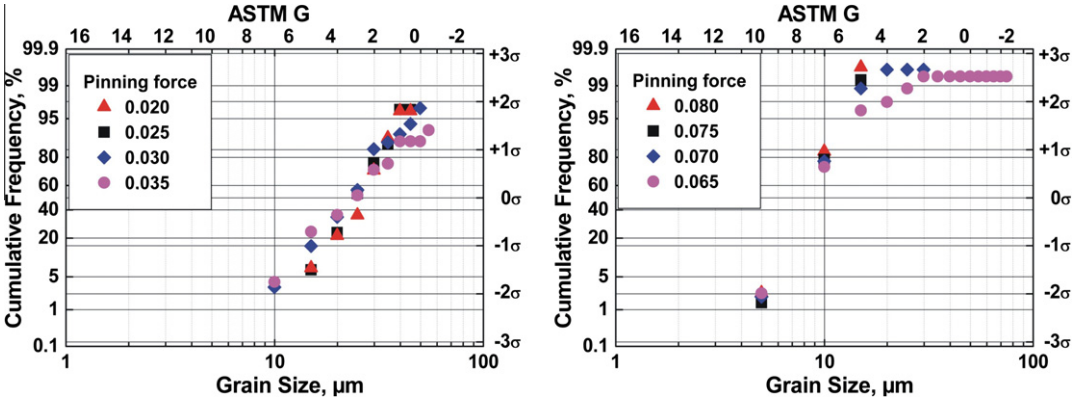

Fig. 5. Grain size distributions for the simulations with varied pinning force.

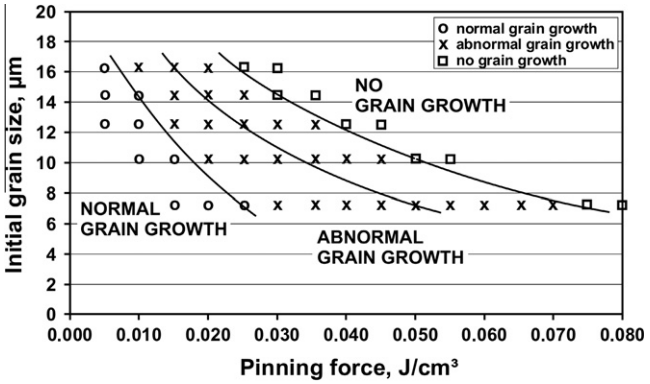

Fig. 6. The various grain-growth regimes as a function of initial grain size and pinning force.

20MnCr5B + Nb and 16MnCr5 + Nb/Ti. The chemical composition of these steels, presented in Table 1, are based on the standard chemical composition of case-hardening steels but with the addition of Nb and Nb + Ti respectively. The consideration is that by means of microalloying elements it is possible to gain sufficient mechanical properties concerning toughness and strength in spite of high-temperature carburising.

The pinning forces for these steels were calculated from the volume fractions of precipitates and their radii. Generally, the volume fraction of precipitates as well as particle radius can be obtained by experiment or by simulation. In this study, the mean particle radii were obtained from TEM-analysis and the volume fraction was calculated by Thermo-Calc®, assuming that all microalloying precipitates were already formed. Because TiN and BN were not found in the TEM-analysis, these precipitates were not included in the calculation of volume fraction and therefore, in the pinning force. The stability of AlN depends on the amount of Al and N. For the investigated steels, it means that at 1050 °C for the 20MnCr5B + Nb, AlN is stable, whereas for the 16MnCr5 + Nb/Ti, it is completely soluble. Thus, for the first steel, NbC and AlN whereas for the second, only NbC were considered in the Thermo-Calc® calculations that affect the different volume fractions and therefore the pinning forces. Table 2 summarizes the results for the calculated volume fractions of precipitates and the measured particle radii, as well as the obtained pinning forces for the selected steels. In addition, the mean initial grain sizes for the two investigated steels were obtained by the linear intercept method (Table 2).

According to Fig. 6, one of the investigated steels, 20MnCr5B + Nb, corresponded to the case of no-grain growth and the second, i.e. 16MnCr5 + Nb/Ti, to abnormal grain growth. There is a good correlation with the experimental results shown in Fig. 7. The characterisation of experimental grain size distributions after carburising is performed according to the specification ZFN 5016, which is defined by ZF Friedrichshafen AG and shows possible limits for grain size in carburised components [18]. The sample of 20MnCr5B + Nb after carburising at 1050 °C does not show abnormal grain growth and the distribution remains below ZFN 5016 specifications. In contrast, the microstructure of 16MnCr5 + Nb/Ti is not maintained in this norm. Signs of abnormal grain growth areas are obvious (Fig. 7).

Table 2
Calculated volume fraction in Thermo-Calc®, measured particle size and pinning force of the selected steels as well as initial grain size.

Steel	Volume fraction Thermo-Calc	Particle radius (nm) TEM	Initial grain size, µm metallography	Pinning force (J/cm³) Eq. (1.2)
20MnCr5B + Nb	0.00124541	23	8	0.065
16MnCr5 + Nb/Ti	0.00075365	25	10	0.036

5. Variation of the simulation scenario for abnormal grain growth

To investigate the factors that promote abnormal grain growth, additional calculations that vary the initial grain diameter and the pinning force are compared to one another. The different scenarios are illustrated in Fig. 8 and Table 3.

The initial structures for these six scenarios are achieved with 15-min pre-simulations. These pre-simulations are conducted via MICRESS® and performed on artificial uniform structures with grain diameters of 8 µm for 20MnCr5B + Nb and 10 µm for 16MnCr5 + Nb/Ti. In the first four pre-simulations, which reflect slow heating to carburising temperature, the calculated and reduced pinning forces of 20MnCr5B + Nb and 16MnCr5 + Nb/Ti from Table 3 are inserted. To create coarse homogeneous structures for the calculation of scenarios 5 and 6, lower pinning forces of 0.025 and 0.020 J/cm³, respectively, are used in the pre-simulations (Fig. 9).

In scenarios 2 and 4, large grain diameters are achieved in the pre-simulations and the structure also becomes inhomogeneous because some grains are much larger in diameter in comparison to the mean diameter. The same is true for scenarios 5 and 6, where coarser structures are obtained than in the other scenarios. Table 3 summarizes simulation scenarios for the following simulations as well as the resulting positions in the grain growth map from Fig. 6.

In the simulations for scenarios 1 and 2 of 20MnCr5B + Nb and 16MnCr5 + Nb/Ti, the calculated pinning force is combined with a fine structure that reflects a possible local situation in the material (Figs. 10 and 11). This can be considered as critical structure due to high driving force for the grain growth because of small grain diameter. The first scenario is related to the upper boundary, where no-grain growth is expected, and the second to the critical boundary, where abnormal grain growth is likely to occur.

The result for the 20MnCr5B + Nb confirms that a pinning force of 0.065 J/cm³ combined with a critical structure does not lead to abnormal grain growth. The structure after 60 min annealing at 1050 °C completely reflects the initial structure, which is consistent with the point at which 20MnCr5B + Nb reaches the upper boundary of the no-grain growth region (Fig. 6). In contrast, the simulation of 16MnCr5 + Nb/Ti with the critical structure leads to explicit abnormal grain growth, where only few grains grow at the expense of others. Two steps in the grain size distribution of the simulation confirm the abnormal grain growth for the second scenario (Fig. 11).

As the pinning force can vary locally, due to an inhomogeneous distribution of particles and later, because of changes during car-

Table 1
Chemical composition of selected steels, mass contents in (%).

Steel	C	Si	Mn	P	S	Cr	Al	B	N	Nb	Ti
20MnCr5B + Nb	0.16	0.22	1.23	0.012	0.027	1.30	0.026	0.003	0.0133	0.034	0.002
16MnCr5 + Nb/Ti	0.18	0.32	1.09	0.013	0.017	1.09	0.011	–	0.0140	0.037	0.026

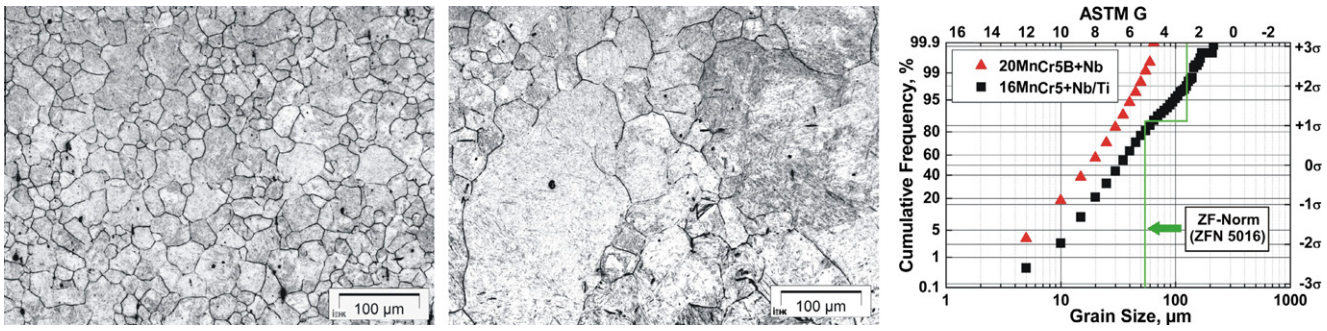

Fig. 7. Micrographs of 20MnCr5B + Nb (left) and 16MnCr5 + Nb/Ti (middle) after carburising at 1050 °C and corresponding grain size distributions obtained by the linear intercept method (right).

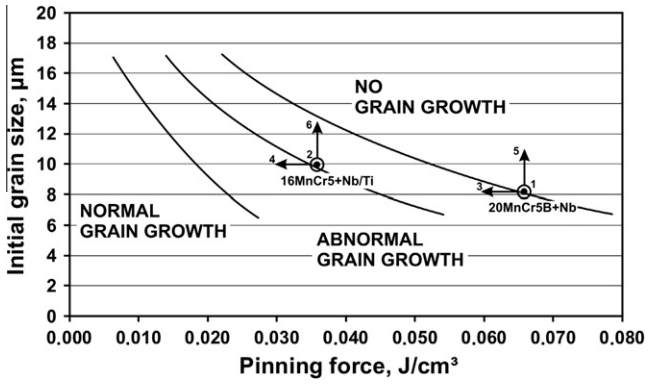

Fig. 8. Parameter variations during grain growth simulations for the steels 20MnCr5B + Nb and 16MnCr5 + Nb/Ti.

burising as a result of particle coarsening, it is of interest to investigate the influence of varying pinning forces. The following two simulations are performed with reduced pinning force. By reducing pinning force, the positions of 20MnCr5B + Nb and 16MnCr5 + Nb/Ti in the grain growth map (Fig. 8) shift to the left, as illustrated by scenarios 3 and 4 in Table 3. The position of 20MnCr5B + Nb moves into the abnormal grain growth area and remains close to the upper boundary. The position of 16MnCr5 + Nb/Ti shifts a little as well, but remains close to the critical boundary because when pinning force decreases, the average grain diameter in the initial structure slightly increases (Fig. 9). The simulation results fully agree with these considerations (Figs. 12 and 13). For 20MnCr5B + Nb, the calculation with critical structure and reduced pinning force leads to the appearance of abnormal grain growth onset. For 16MnCr5 + Nb/Ti, scenario 4 results in a decline in abnormal grain growth, which is, however, still distinct. The tendency to abnormal grain growth in both steels can be derived from the grain

Table 3
Selected simulation scenarios for 20MnCr5B + Nb and 16MnCr5 + Nb/Ti.

Boundary condition	Steel	Pinning force		Initial structure	Position in the grain-growth map
Scenario 1	20MnCr5B + Nb	0.065 J/cm^3	Calculated	Fine	On the upper boundary
Scenario 2	16MnCr5 + Nb/Ti	0.036 J/cm^3	Calculated	Fine	Close to the critical boundary
Scenario 3	20MnCr5B + Nb	0.053 J/cm^3	Reduced	Fine	Left to the upper boundary
Scenario 4	16MnCr5 + Nb/Ti	0.030 J/cm^3	Reduced	Fine	Close to the critical boundary
Scenario 5	20MnCr5B + Nb	0.065 J/cm^3	Calculated	Coarse	In the no-grain growth area
Scenario 6	16MnCr5 + Nb/Ti	0.036 J/cm^3	Calculated	Coarse	In the no-grain growth area

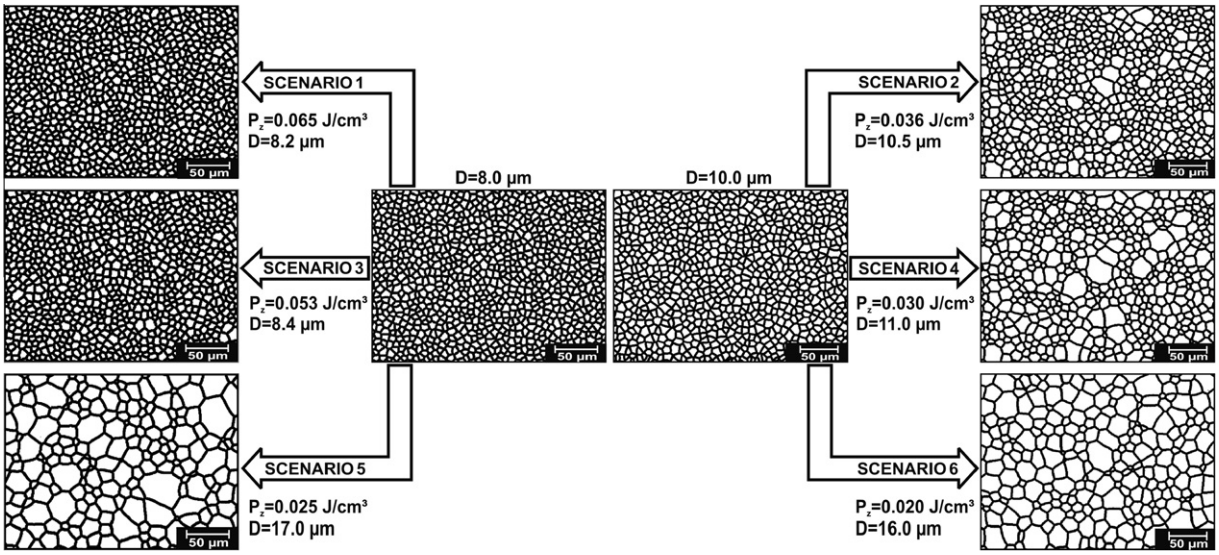

Fig. 9. Grain size pre-calculations in order to create quasi-real microstructures with defined grain size which afterwards have been used as initial microstructure for the grain evolution calculation during carburising with relation to the scenarios 1–6; this pre-calculation describes the effect of heating.

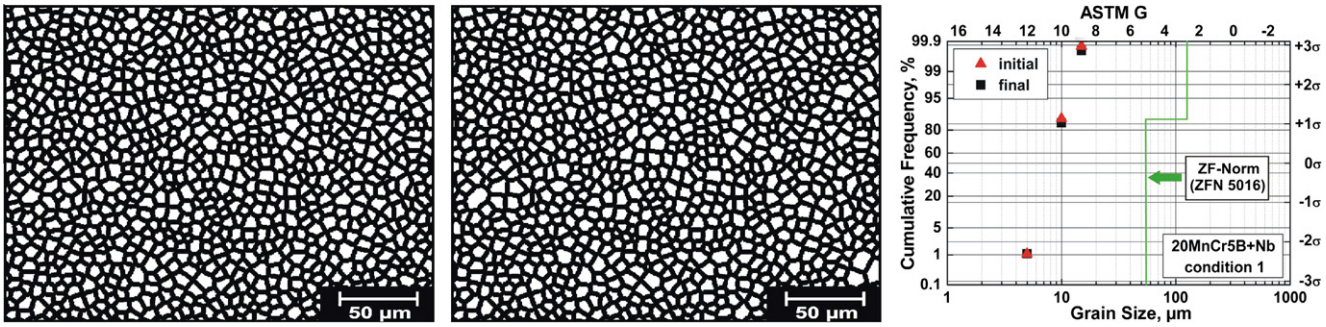

Fig. 10. Initial and final microstructure after 60 min annealing at 1050 °C as well as grain size distributions corresponding to scenario 1.

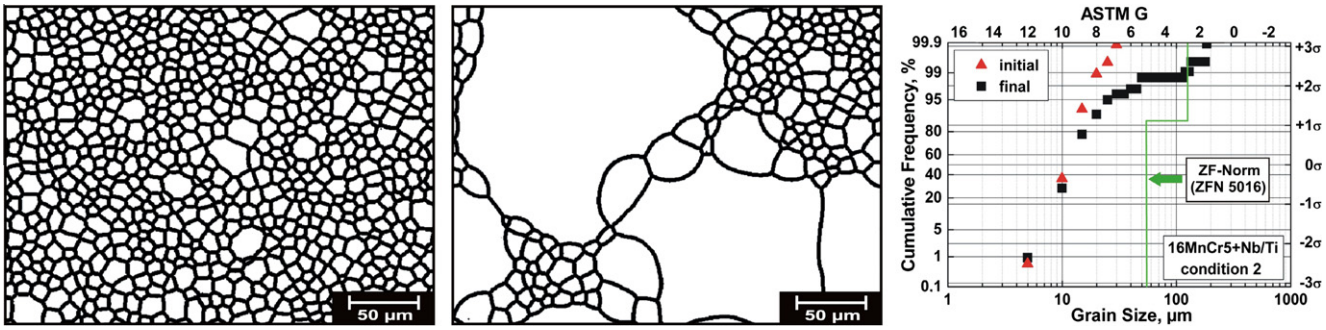

Fig. 11. Initial and final microstructure after 60 min annealing at 1050 °C as well as grain size distributions corresponding to scenario 2.

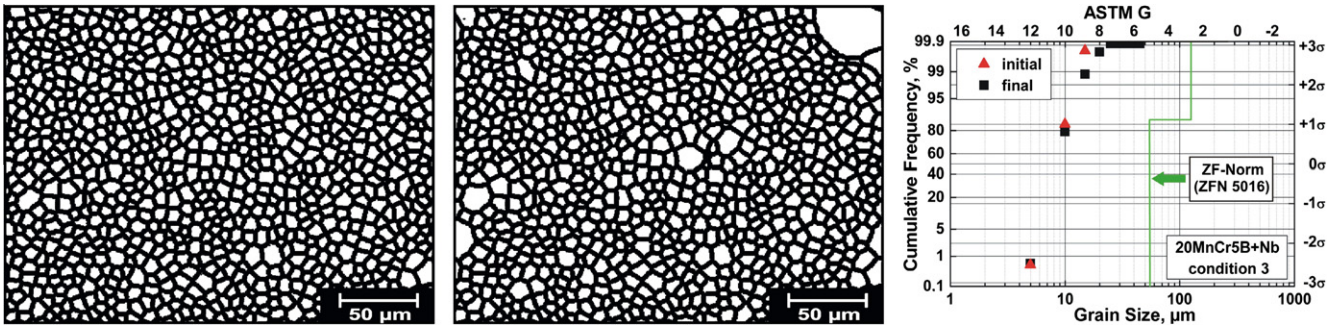

Fig. 12. Initial and final microstructure after 60 min annealing at 1050 °C as well as grain size distributions corresponding to scenario 3.

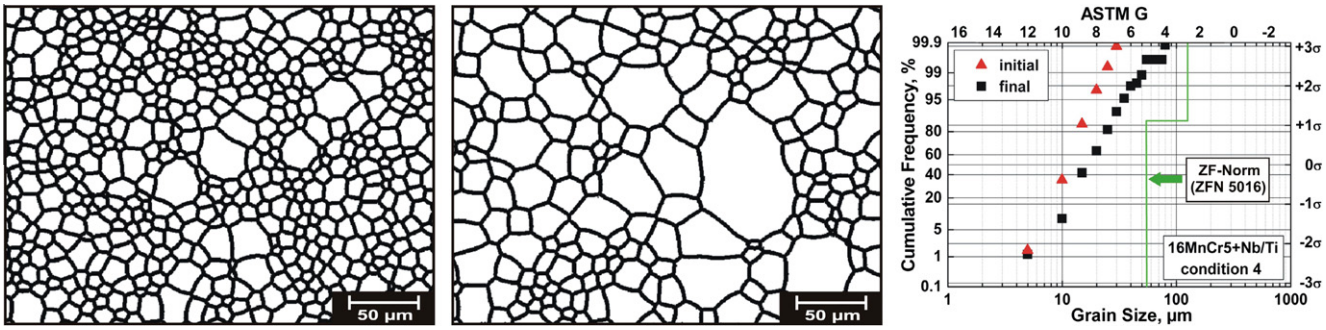

Fig. 13. Initial and final microstructure after 60 min annealing at 1050 °C as well as grain size distributions corresponding to scenario 4.

size distributions. Thus, the critical initial structures lead to completely different microstructure evolutions if the pinning force has other values.

Typically, the real microstructure is inhomogeneous and presents a composition of areas with small and coarse grains. The grain growth behaviour in the fine-grain area was explored in scenarios 1–4. In the case of a coarse-grain area in the initial structure, grain growth occurs differently, even if the same pinning force is available. In (Figs. 14 and 15), the results of scenarios 5 and 6 are presented.

It is obvious that scenarios 5 and 6 do not lead to abnormal grain growth. This can be explained by the lower driving force that is the consequence of coarse initial structure. In the calculations, there is only a slight change of grain size due to microstructure sta-

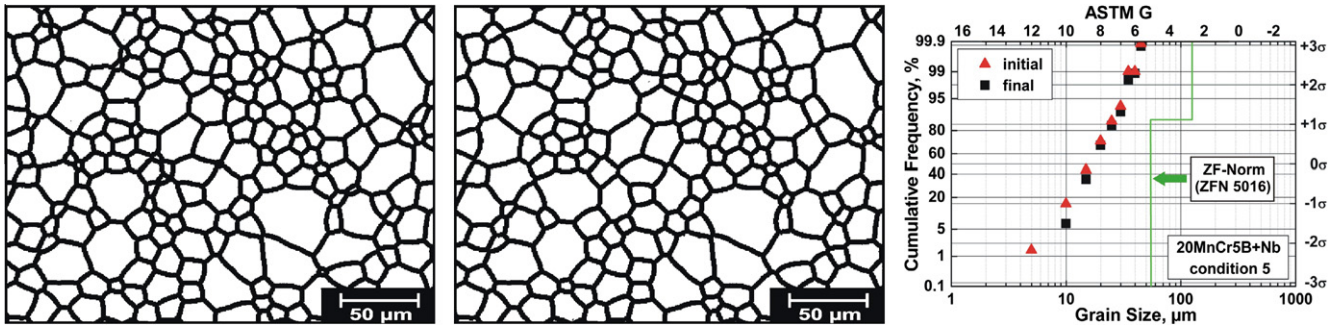

Fig. 14. Initial and final microstructure after 60 min annealing at 1050 °C as well as grain size distributions corresponding to scenario 5.

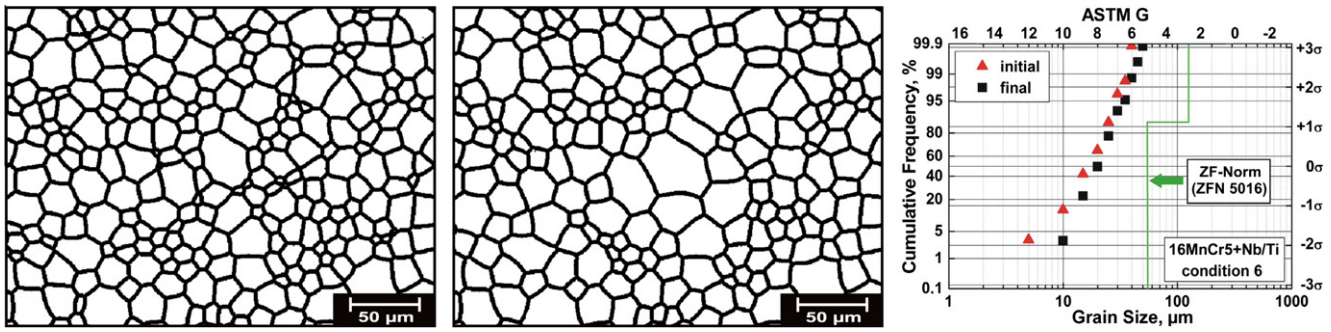

Fig. 15. Initial and final microstructure after 60 min annealing at 1050 °C as well as grain size distributions corresponding to scenario 6.

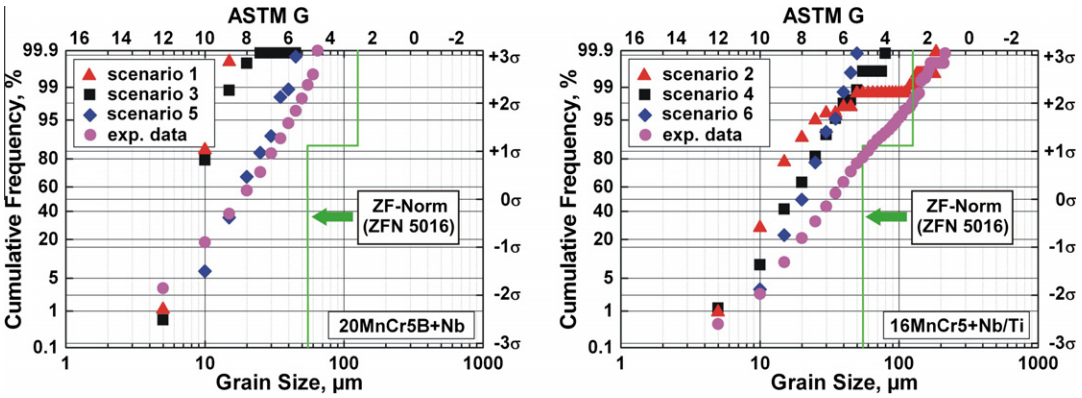

Fig. 16. Simulated grain size distributions for the scenarios from Table 3 compared to the experimental results for 20MnCr5B + Nb and 16MnCr5 + Nb/Ti.

bilisation. Again, the results correspond with the position in the no-grain growth area.

Fig. 16 summarizes the simulation results for all selected scenarios from Table 3 and the experimentally detected grain size distributions. The experimental outcome for both steels is qualitatively in agreement with the simulation results, as the determination of the grain growth type corresponds. The reason for the difference in the experimental and simulation data is due to the fact that in the calculation, ideal microstructures are used, whereas the real structure is usually a combination of small and big grains. By using different combinations of pinning force and initial structures, different local situations of real structures can be simulated. Accordingly, it can be assumed that carburising does not encourage a great deal of abnormal grain growth in 20MnCr5B + Nb, although this steel does show the onset of abnormal grain growth. However, the grain size distribution is below ZFN 5016 specifications and therefore acceptable. In contrast, the combination of critical pinning force and critical arrangement of grains (scenarios 2 and 4) in the initial structure leads to abnormal grain growth in steel 16MnCr5 + Nb/Ti.

In conclusion, the pinning force is not the only important factor in the evolution of grain size. The critical combination of pinning force and initial microstructure, i.e. average grain size, leads to abnormal grain growth. Additionally, it should be mentioned that besides the initial grain size, the grain vicinity may be important in determining whether and in which manner a grain grows. The influence of this parameter was not studied here but should be examined in the future. The grain boundary mobility also influences microstructure evolution. However, this parameter only affects the time scale and does not have an influence on grain growth character.

6. Conclusions

A rigorous numerical approach using the phase-field method for the prediction of microstructure evolution has been developed. It is demonstrated that the increase of pinning force leads to a change in the grain growth character. Moreover, the initial grain size strongly influences grain growth behaviour.

The model is actually able to predict abnormal grain growth as well as local grain size distributions. The components of an exact prediction of a grain size distribution is not yet possible, because the local distribution of grain size, the local concentration of precipitates and their change in size during processing remain unknown. However, the model can be successfully used for material and process design, i.e. if chemical composition, initial grain size and process parameters are known, information can be derived about grain growth behaviour. Simulations with possible critical conditions reveal if abnormal grain growth will occur or not. In the future, the model can be improved by considering the particle and the initial grain size distribution as input data instead of the mean particle or mean grain size, as well as by using a variable pinning force according to the evolution of precipitation size and distribution.

Acknowledgement

The essential work for modelling high-temperature carburisation was done in the project Carbain (RFSR-CT-2004-00028) which is greatly funded by the European Commission [19].

References

[1] B.R. Patterson, Y. Liu, Metall. Trans. 23A (1992) 2481–2482.
[2] K.A. Alogab, D.K. Matlock, J.G. Speer, H.J. Kleebe, ISIJ Int. 47 (2007) 307–316.
[3] T. Gladman, JOM 44 (1992) 21–24.
[4] T. Gladman, Grain Size Control. Charlesworth Group, 2004. ISBN:1 904350 22 4.
[5] F.J. Humphreys, Acta Mater. 45 (1997) 5031–5039.
[6] F.J. Humphreys, M. Hatherly, Recrystallization and Related Annealing Phenomena, first ed., Gillard (Printers) Ltd., Great Yarmouth, 1995. ISBN:0 08 041884 8.
[7] M. Hillert, Acta Metall. 13 (1965) 227–238.
[8] D.J. Srolovitz, G.S. Grest, M.P. Anderson, Acta Metall. 34 (1986) 1833–1845.
[9] M.P. Anderson, G.S. Grest, D.J. Srolovitz, Philos. Mag. B 59 (1989) 293–329.
[10] T. Murakami, H. Hatano, H. Yaguchi, Tetsu-to-Hagané. 92 (2006) 38–46.
[11] D.A. Porter, K.E. Easterling, Phase Transformations in Metals and Alloys, 2004.
[12] ACCESS e.V.: MICRESS® User Documentation, Version 5.01, 2004. <www.MICRESS.de>.
[13] I. Steinbach, F. Pezzolla, B. Nestler, M. Seeßelberg, R. Prieler, G.J. Schmitz, J.L.L. Rezende, Phys. D 94 (1996) 135–147.
[14] B. Böttger, M. Apel, J. Eiken, P. Schaffnit, I. Steinbach, Steel Res. Int. 79 (2008) 608–616.
[15] I. Steinbach, M. Apel, Dual scale simulation of grain growth using a multiphase-field model, in: Advances in Materials Theory and Modeling – Bridging Over Multiple-Length and Time. MRS Spring Meeting, 2001, pp. AA7.14.1–AA7.14.6.
[16] M. Apel, B. Böttger, J. Rudnizki, P. Schaffnit, I. Steinbach, ISIJ Int. 49 (2009) 1024–1029.
[17] R.G. Thiessen, Physically-Based Modelling of Material Response to Welding, Ph.D. Thesis, TU-Delft, 2006.
[18] ZF Friedrichshaven AG: ZFN 5016 – Korngrößenbestimmung bei Einsatz- und Vergütungstählen, Company Specification, 1994.
[19] RFSR-CT-2004-00028: New Ecological and low Cost Answers to End-User Demands on High Performance Steel Components, Research Program of the Research Fund for Coal and Steel, 2008.